Energetic Diurnal Tides Along the Oregon Coast

J. J. Osborne, * A. L. Kurapov, G. D. Egbert, and P. M. Kosro

College of Earth, Ocean, and Atmospheric Sciences, Oregon State University

*Corresponding author address: John Osborne, College of Earth, Ocean, and Atmospheric Sciences, Oregon State University, 104 CEOAS Administration Building, Corvallis, OR 97331.

E-mail: josborne@coas.oregonstate.edu

ABSTRACT

Diurnal tides are found to be anomalously strong along portions of the Oregon shelf (US west coast), based on analyses of data and outputs of a 1-km resolution ocean circulation model. Intensified K_1 tidal currents (0.07 m s^{-1}) over a wider part of the shelf (44°N – 44.5°N), previously predicted by Erofeeva et al. (2003), are confirmed here by newly available high-frequency (HF) radar surface current data. However, these magnitudes are dwarfed compared to the 0.4 m s^{-1} diurnal tidal currents near Cape Blanco (43°N), found in the model and HF radar data. There, tidal variability dominates the relative vorticity spectrum, suggesting that tides may contribute to separation of the coastal current at that location. Intensified diurnal tides are also found near other capes resolved by the model. These dynamics will have to be considered when decisions are made about establishing Marine Reserves/Protected Areas for fish larvae retention.

1. Introduction

Summer circulation off the Oregon coast is characterized by wind-driven coastal upwelling varying on temporal scales of several days, driving a southward jet with mean speed of 0.5 m s^{-1}. As summer progresses, the cold sea surface temperature (SST) front (Figure 1a) is driven offshore by Ekman transport, eddy variability, and separating coastal jets. Tides are dominated by the M_2 constituent (period of 12.42 hr), with barotropic (depth-averaged) currents of up to 0.06 m s^{-1} over the shelf and internal tides reaching 0.15 m s^{-1} (Hayes and Halpern 1976; Torgrimson and Hickey 1979; Erofeeva et al. 2003; Kurapov et al. 2003; Osborne et al. 2011). Other tidal constituents are generally weak, with the possible exception of K_1 (period of 23.93 hr). Using a two-dimensional data-assimilating ocean tide model, Erofeeva et al. (2003) suggested that K_1 tidal currents could exceed 0.10 m s^{-1} over the widest portion of the Oregon shelf ($44°\text{N} - 44.5°\text{N}$).

While tidal currents are usually less energetic than wind-driven currents in this region, our recent model results using a comprehensive three-dimensional coastal ocean model (described in section 2) reveal that the shape of the SST front is sensitive to barotropic tidal forcing (Figure 1b-d). While all model solutions qualitatively reproduce observed seasonal upwelling, front geometry varies between cases using atmospheric forcing only (Figure 1b), atmospheric forcing plus M_2 tides on the open boundaries (Figure 1c), or atmospheric forcing plus eight tidal constituents (M_2, S_2, K_2, N_2, K_1, O_1, P_1, and Q_1) (Figure 1d). While differences in the SST front geometry may possibly reflect the high sensitivity of the non-linear hydrostatic model to small changes in the boundary conditions (Oliger and Sundstrom 1978), it is also possible that tides contribute to eddy dynamics at subtidal time scales in some deterministic fashion, which affects offshore transport. To explore this possibility, we focus on shelf flows, finding strong observed and modeled diurnal currents in the area identified by Erofeeva et al. (2003) (section 3) and even stronger diurnal currents near Cape Blanco (42.8°N; section 4).

2. Model

The model used here is based on the Regional Ocean Modeling System (ROMS, Shchepetkin and McWilliams (2005), www.myroms.org) a non-linear, hydrostatic, Boussinesq model. Details of implementation are very similar to Osborne et al. (2011). Resolution is 1 km in the horizontal and 40 terrain-following levels in the vertical, over realistic bathymetry. The study period is April through August 2002. In each case considered, winds are daily averages from the Coupled Ocean Atmosphere Mesoscale Prediction System (COAMPS; Hodur 1997) and parameters for surface heat flux computation are monthly averages from the National Centers for Environmental Prediction (NCEP) reanalysis (Kalnay et al. 1996). Subtidal boundary conditions come from a 3−km regional ocean circulation model (Koch et al. 2010) and barotropic tides are from a 1/30° regional data-assimilating model (Egbert and Erofeeva 2002, http://volkov.oce.orst.edu/tides/). Three cases have been considered, differing in the barotropic tidal forcing along the open boundaries: "winds only" (case WO, Figure 1b), winds and M_2 tides (case W+M_2, Figure 1c), and winds and eight tidal constituents (case TW; Figure 1d). Case W+M_2 has been discussed at length by Osborne et al. (2011). Unless specifically mentioned, results from case TW are discussed here.

3. Intensified K_1 Tides Observed by High Frequency Radars

Erofeeva et al. (2003) noted local intensification of K_1 currents over the broader portion of the Oregon shelf between 44°−44.5°N (Heceta and Stonewall Banks) in a data-assimilating model of barotropic tides on the Oregon coast, which was interpreted as an effect of a coastal trapped wave resonant over the local shelf bathymetry. In their study, surface velocities from short range (40 km) high frequency (HF) radars were assimilated, but these data did not did not extend to the high-energy region, hence no direct observational evidence was available at

that time to confirm intensification of the modeled K_1 tides. Surface current data from two long range (150 km) HF radars with overlapping coverage are now available in this region (Figure 2; Kosro 2005; Kosro et al. 2006; Saraceno et al. 2008), at 43.75°N (Winchester Bay, WIN) and at 44.7°N (Yaquina Head Long, YHL). We analyze observations from WIN for June-July 2002 and observations from YHL (installed later) for June-July 2008. While the YHL observations are not from the same year as our model, the diurnal tide (mostly barotropic) is believed to be fairly independent of background hydrographic conditions, so there should still be agreement between the two different years. Note each radar measures the radial component of the currents, in the direction to/from each radar.

To isolate the K_1 signal, HF radar radial velocity component measurements have been high-pass filtered (with a 40-hr half-amplitude filter) and harmonically analyzed at the K_1 frequency. The resulting harmonic amplitudes are plotted in Figure 2a (YHL) and Figure 2b (WIN). The observations between 44°N and 45°N show large areas with radial currents above 0.05 m s^{-1} and peak amplitudes of 0.10 m s^{-1} (YHL) and 0.07 m s^{-1} (WIN). Radial current amplitudes from YHL and WIN over the shelf near 44.5°N differ due to the polarization of K_1 tidal currents, which are mostly north-south at this location, nearly orthogonal to the radial component of the YHL radar, but more directly along the radial component of the WIN radar. To compare our model solution to HF radar observations, model surface current velocities are first projected in the direction of HF radials and are then high-pass filtered and harmonically analyzed. Both model and HF radar radial component velocity estimates qualitatively agree with each other, as well as with the data-assimilating barotropic tidal model of Erofeeva et al. (2003).

4. Intensified Diurnal Tides Around Capes

In addition to amplified K_1 currents over the wider shelf area, the WIN radar shows strong K_1 tides off Cape Arago (43.3°N, see Figures 2b,d). These amplitudes are as large as those

between 44°N and 45°N. To gain additional perspective on K_1 tides on the entire Oregon shelf, the root mean square of K_1 tidal current amplitudes, RMSA $= \sqrt{(\tilde{u}^2 + \tilde{v}^2)/2}$, are computed for the shelf area during June and July 2002 (Figure 3a), where $\tilde{u}, \tilde{v}$ are harmonic constants of modeled K_1 surface currents. In addition to the areas mentioned above, strong K_1 tides are also found at several spots between 41.5°N and 43.5°N, particularly near coastal capes. At Cape Blanco (42.8°N), RMSA reaches 0.2 m s^{-1}.

The K_1 model estimates are generally consistent with moored acoustic Doppler current profiler (ADCP) measurements collected in the high-energy regions over two different years, including three locations from the 2001 Coastal Ocean Advances in Shelf Transport (COAST) experiment (Boyd et al. 2002) between 44°N and 45°N (positions marked with stars, Figure 3) and two locations to the north (43.2°N) and south (42.4°N) of Cape Blanco, from the 2002 Global Ocean Ecosystem Dynamics (GLOBEC) program (Batchelder et al. 2002; Ramp and Bahr 2008). The RMSA shown in boxes in Figure 3 correspond to velocity estimates at each ADCP's upper depth bin (10-20 m from surface). At all five moorings, the K_1 tide is found to be nearly depth-independent. Curiously, observed K_1 currents (0.12 m s^{-1}) off of Gold Beach (42.4°N) are appreciably larger than model values (0.04 m s^{-1}) at this exact location, but are comparable to intensified model currents closer to the coast.

For additional insight, harmonically analyzed barotropic (depth-averaged) K_1 modeled tidal currents have been decomposed into counterclockwise (CCW) and clockwise (CW) rotary components, $(\tilde{u} \pm \mathrm{i}\tilde{v})/2$, and their amplitude and phase are shown in Figure 3b,c. In our case, CW amplitudes are generally large where RMSA is large and CCW amplitudes are small everywhere, save at the capes between 41.5°N and 43.5°N. Within a few kilometers of the capes, horizontal current ellipses are linearly polarized, with the direction of velocity vector rotation poorly defined. There, maximum CCW and CW amplitudes are approximately equal, up to 0.10 m s^{-1}. CW rotary current phase shows northward wave propagation over the shelf between 42.5°N and 44.75°N and also between 41.5°N and 42°N. This is generally consistent with the analysis of Erofeeva et al. (2003), which showed northward phase

propagation of CW rotary currents between 43.5°N and 45°N.

Intensification of diurnal tidal currents between 41.5°N and 43.5°N may result from a combination of two mechanisms. First, general intensification may be due to a continental shelf wave, like those reported at St. Kilda, UK (Cartwright 1969), Vancouver Island, Canada (Crawford and Thomson 1982), in many locations in the Sea of Okhotsk (Kovalev and Rabinovich 1980; Yefimov and Rabinovich 1980; Rabinovich and Zhukov 1984; Odamaki 1994; Rabinovich and Thomson 2001), and, of course, over Heceta Bank (Erofeeva et al. 2003). Second, the particularly large amplitudes within a few kilometers of capes may result from flow constriction over shallow bathymetry and around the capes.

Data from a high-frequency radar located at the tip of Cape Blanco (124.57°W, 42.84°N) confirm strong diurnal tides. A twenty-day time series of high-pass filtered HF radial component velocity at a point off Cape Blanco (inset in Figure 5b) is shown in Figure 4 (black line). Here, currents may exceed 0.40 m s^{-1} and vary up to 0.75 m s^{-1} over the course of a day. Modeled currents are very similar in amplitude and phase (Figure 4, gray line). Larger currents are generally found when K_1 and O_1 are in phase, e.g., during periods of diurnal spring tides. The period of the diurnal spring tide is 13.58 days, about 1 day less than the 14.88 day period of the M_2-S_2 spring-neap cycle.

Events of intensified M_2 tide may also be identified in this area. They are intermittent, associated with internal tide motions, and less predictable than diurnal tides. An area of strong barotropic-to-baroclinic M_2 tide conversion is predicted on the continental slope at a distance of 60 km to the southwest of the cape (Osborne et al. 2011) and is influencing events here.

In addition to being a site with strong tides, Cape Blanco is a separation point of the equatorward coastal jet (Barth et al. 2000). Energetic tides here may contribute to eddy dynamics and modify cross-shelf transport. Figure 5a shows time series of model-derived relative vorticity normalized by the Coriolis parameter, $f^{-1}(\partial v/\partial x - \partial u/\partial y)$, in cases TW (gray) and WO (black) at the same point and during the same time as the radial velocity

time series in Figure 4. Case TW shows periodic high-frequency variability in the normalized vorticity with peak values exceeding 2, suggesting strongly non-linear flows. Vorticity spectra (Figure 5b) confirm that case TW (gray) has significantly more power (at the 95% confidence level) at higher frequencies than case WO (black), with peaks appearing at one and two cycles per day, corresponding to diurnal and semi-diurnal tides.

5. Summary

High frequency radar observations confirm the presence of intensified K_1 tides in the region between 44°N and 44.5°N, as in the data-assimilating shallow-water model of Erofeeva et al. (2003). Our model solution and the observations also show strong diurnal tidal currents around several capes on the Oregon coast, most notably at Cape Blanco, where tidal current speeds may reach 0.4 m s^{-1}. These tidal currents are largest during periods of K_1-O_1 spring tides and are accurately predicted by the model. Semi-diurnal tides also contribute to variability off Cape Blanco. Both diurnal and semi-diurnal tides alter relative vorticity in this area. Finally, there is potential for strong tides to enhance vertical mixing and particle dispersion along the coast. Pilot and planned marine reserves and protected areas (boxed regions, Figure 3) have been chosen, in part, as areas of high larvae retention rates. Numerical simulations of larvae dispersion (e.g., Kim and Barth (2011)) must begin to account for tidal variability to more accurately predict particle movement and retention.

Acknowledgments.

This research was supported by the National Science Foundation (Grants OCE-0000734, OCE-0648314, and OCE-1030922), the Office of Naval Research Physical Oceanography Program (Grants N000140810942 and N000141010745), National Oceanic and Atmospheric Administration (NOAA) grant NA11NOS0120036, NOAA-CIOSS, and NOAA-IOOS (NANOOS). The authors thank J. A. Barth, M. S. Hoecker-Martinez, and S. H. Suanda for their helpful

discussions.

REFERENCES

Barth, J. A., S. D. Pierce, and R. L. Smith, 2000: A separating coastal upwelling jet at Cape Blanco, Oregon and its connection to the California Current System. *Deep-Sea Research II*, **47**, 783–810.

Batchelder, H. P., et al., 2002: The GLOBEC Northeast Pacific California Current System program. *Oceanography*, **15**, 36–47.

Boyd, T., M. D. Levine, P. M. Kosro, S. R. Gard, and W. Waldorf, 2002: Observations from Moorings on the Oregon Continental Shelf, May - August 2001. Data Report 190, Oregon State University, College of Oceanic and Atmospheric Sciences, 104 Ocean Admin Bldg, Corvallis, OR 97331.

Cartwright, D. E., 1969: Extraordinary tidal currents near St. Kilda. *Nature*, **223**, 928–932.

Crawford, W. R. and R. E. Thomson, 1982: Continental shelf waves of diurnal period along Vancouver Island. *Journal of Geophysical Research*, **87 (C12)**, 9516–9527.

Egbert, G. D. and S. Y. Erofeeva, 2002: Efficient inverse modeling of barotropic ocean tides. *Journal of Atmospheric and Oceanic Technology*, **19 (2)**, 183–204.

Erofeeva, S. Y., G. D. Egbert, and P. M. Kosro, 2003: Tidal currents on the central Oregon shelf: Models, data and assimilation. *Journal of Geophysical Research*, **108**, 3148, doi:10.1029/2002JC001615.

Hayes, S. P. and D. Halpern, 1976: Observations of internal waves and coastal upwelling on the Oregon coast. *Journal of Marine Research*, **34**, 247–267.

Hodur, R. M., 1997: The Naval Research Laboratory's Coupled Ocean/Atmosphere Mesoscale Prediction System (COAMPS). *Monthly Weather Revuew*, **125**, 1414–1430.

Kalnay, E., et al., 1996: The NCEP/NCAR 40-year reanalysis project. *Bulletin of the American Meterological Society*, **77 (3)**, 437–471.

Kim, S. and J. A. Barth, 2011: Connectivity and larval dispersal along the Oregon coast estimated by numerical simulations. *Journal of Geophysical Research*, **116**, L06 002, doi:10.1029/2010JC006741.

Koch, A. O., A. L. Kurapov, and J. S. Allen, 2010: Near-surface dynamics of a separated jet in the coastal transition zone off Oregon. *Journal of Geophysical Research*, **115**, C08 020, doi:10.1029/2009JC005704.

Kosro, P. M., 2005: On the spatial structure of coastal circulation off Newport, Oregon, during spring and summer 2001, in a region of varying shelf width. *Journal of Geophysical Research*, **110**, C10S06, doi:10.1029/2004JC002769.

Kosro, P. M., W. T. Peterson, B. M. Hickey, R. K. Shearman, and S. D. Pierce, 2006: The physical vs. the biological spring transition: 2005. *Geophysical Research Letters*, **33 (22)**, L22S03, doi:10.1029/2006GL027072.

Kovalev, P. D. and A. B. Rabinovich, 1980: Bottom measurements of tidal currents in the southern part of the Kuril-Kamchatka trench. *Oceanology*, **20**, 294–299.

Kurapov, A. L., G. D. Egbert, J. S. Allen, , R. N. Miller, S. Y. Erofeeva, and P. M. Kosro, 2003: The M_2 internal tide off Oregon: Inferences from data assimilation. *Journal of Physical Oceanography*, **33**, 1733–1757.

Maturi, E., A. Harris, C. Merchant, J. Mittaz, B. Potash, W. Meng, and J. Sapper, 2008: NOAA's sea surface temperature products from operational geostationary satellites. *Bulletin of the American Meteorological Society*, **89 (12)**, 1877–1888.

Odamaki, M., 1994: Tides and tidal currents along the okhotsk coast of Hokkaido. *J. Oceanogr.*, **50**, 265–279.

Oliger, J. and A. Sundstrom, 1978: Theoretical and practical aspects of some initial boundary value problems in fluid dymaics. *SIAM J. Appl. Math.*, **35**, 419–446.

Osborne, J. J., A. L. Kurapov, G. D. Egbert, and P. M. Kosro, 2011: Spatial and temportal variaiblity of the m_2 internal tide generation and propagation on the Oregon shelf. *J. of Phys. Oceanogr.*, 2037–2062, doi:10.1175/JPO-D-11-02.1.

Rabinovich, A. B. and R. E. Thomson, 2001: Evidence of diurnal shelf waves in satellite-tracked drifter trajectories off the Kuril Islands. *J. Phys. Oceanogr.*, **31**, 2650–2668.

Rabinovich, A. B. and A. E. Zhukov, 1984: Tidal oscillations on the shelf of Sakhalin Island. *Oceanology*, **24**, 184–189.

Ramp, S. R. and F. L. Bahr, 2008: Seasonal evolution of the upwelling process south of Cape Blanco. *Journal of Physical Oceanography*, **38**, 3–28.

Saraceno, M., P. T. Strub, and P. M. Kosro, 2008: Estimates of sea surface height and near surface alongshore coastal currents from combinations of altimeters and tide gauges. *Journal of Geophysical Research*, **113**, C11 013, doi:10.1029/2008JC004756.

Shchepetkin, A. F. and J. C. McWilliams, 2005: The regional oceanic modeling systems (ROMS): a split-explicit, free-surface, topography-following-coordinate oceanic model. *Ocean Modelling*, **9**, 347–404, doi: 10.1016/j.ocemod.2004.08.002.

Torgrimson, G. M. and B. M. Hickey, 1979: Barotropic and baroclinic tides over the continental slope and shelf off Oregon. *Journal of Physical Oceanography*, **9 (5)**, 946–961.

Yefimov, V. V. and A. B. Rabinovich, 1980: Resonant tidal currents and their relation to continental shelf waves of the northwestern Pacific Ocean. *Izv., Atmos. Oceanic Phys.*, **16**, 805–812.

List of Figures

1 August 2002 mean sea surface temperature: (a) GOES satellite observations (Maturi et al. 2008), (b) ROMS model case WO, (c) case W+M_2, and (d) case TW. White lines mark the 200-m isobath. 13

2 Tidal amplitudes of K_1 surface current radial amplitudes from HF radars (left) and model (right). Top panels are for the YHL radar and bottom panels for the WIN radar. Black lines mark the 200-m isobath and the coast. 14

3 (a) K_1 RMSA along the Oregon coast from case TW. Stars mark 2001 (along 44.3°N, 44.75°N) and 2002 (near Cape Blanco) mooring locations, with annotations giving the moorings' K_1 RMSA at their surface-most depth bin. White boxes along the coast at 42.7°N, 44.1 − 44.25°N, 44.75°N , and 45°N mark proposed and pilot marine protected areas and reserves. (b) Counterclockwise rotary current amplitude (shading) and phase (thin lines, every 30°) of depth-averaged K_1 currents. (c) Clockwise rotary current amplitude and phase of depth-averaged K_1 currents. In all panels, the thick black line marks the 200-m isobath. 15

4 Time series of HFR-observed (black) and model (gray) radial velocity component near Cape Blanco (location marked in inset in Figure 5b). 16

5 Upper: Time series of Coriolis-normalized relative vorticity from case WO (black) and case TW (gray) during the same time period from near Cape Blanco. Lower: Spectra of vorticity time series from case WO (black) and case TW (gray), as computed from the entire model run. The 95% confidence interval is shown. Inset: Close-up of Cape Blanco region. Star marks the location of the time series in Figure 4 and this figure. Black lines mark the 50-, 100-, 150-, and 200-m isobaths. 17

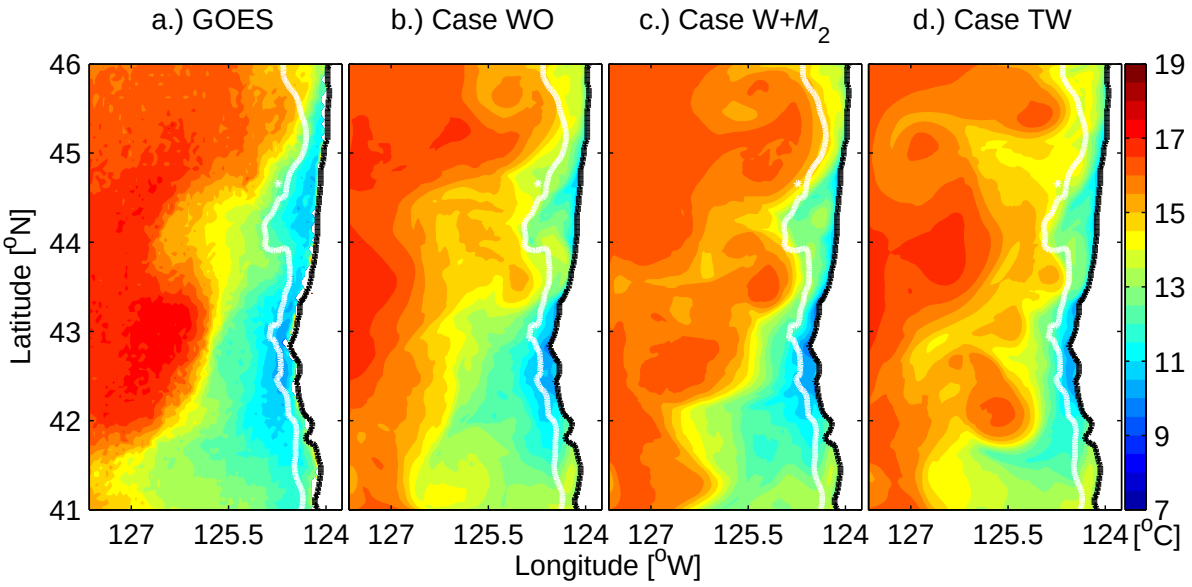

FIG. 1. August 2002 mean sea surface temperature: (a) GOES satellite observations (Maturi et al. 2008), (b) ROMS model case WO, (c) case W+M_2, and (d) case TW. White lines mark the 200-m isobath.

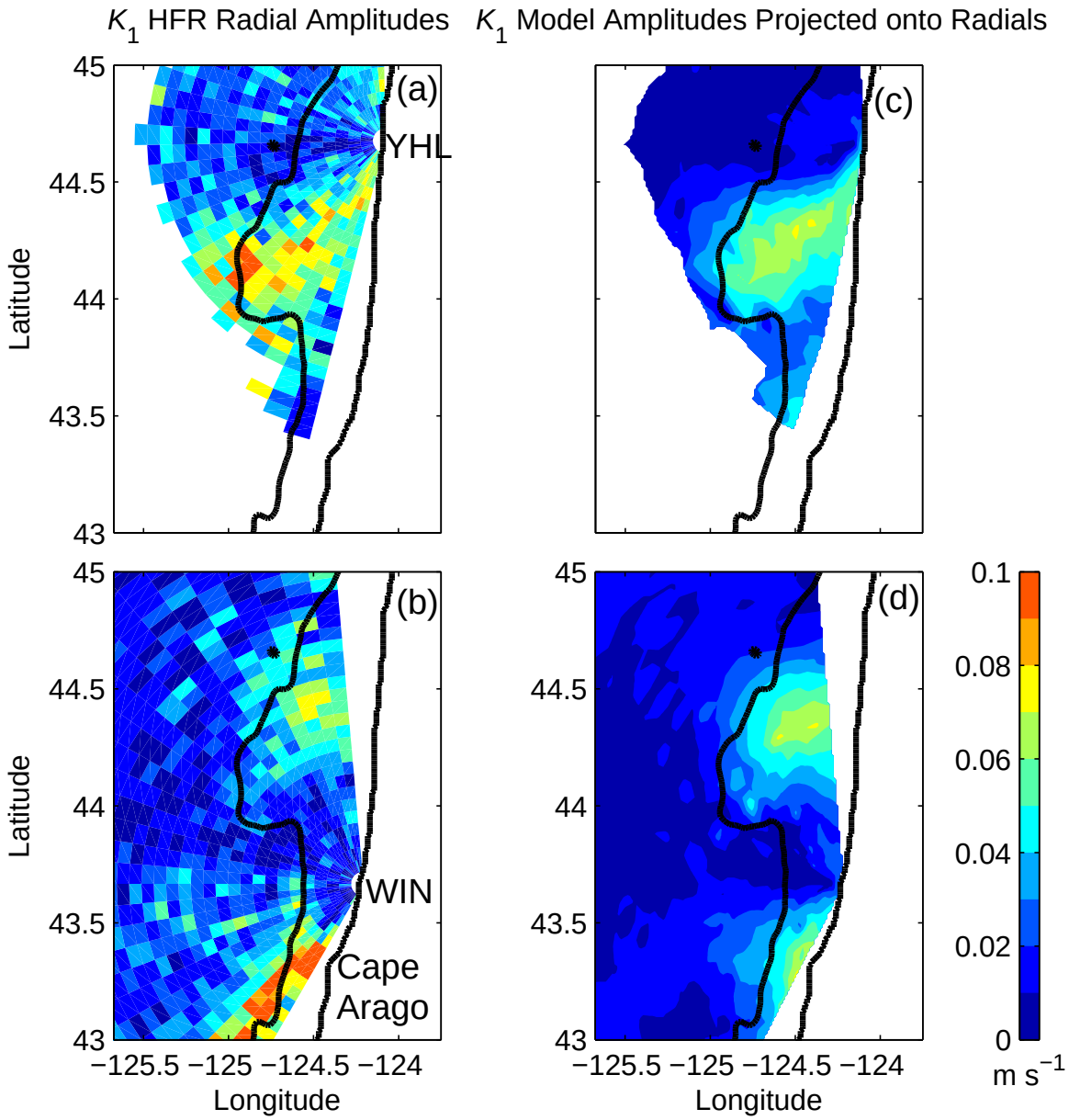

FIG. 2. Tidal amplitudes of K_1 surface current radial amplitudes from HF radars (left) and model (right). Top panels are for the YHL radar and bottom panels for the WIN radar. Black lines mark the 200-m isobath and the coast.

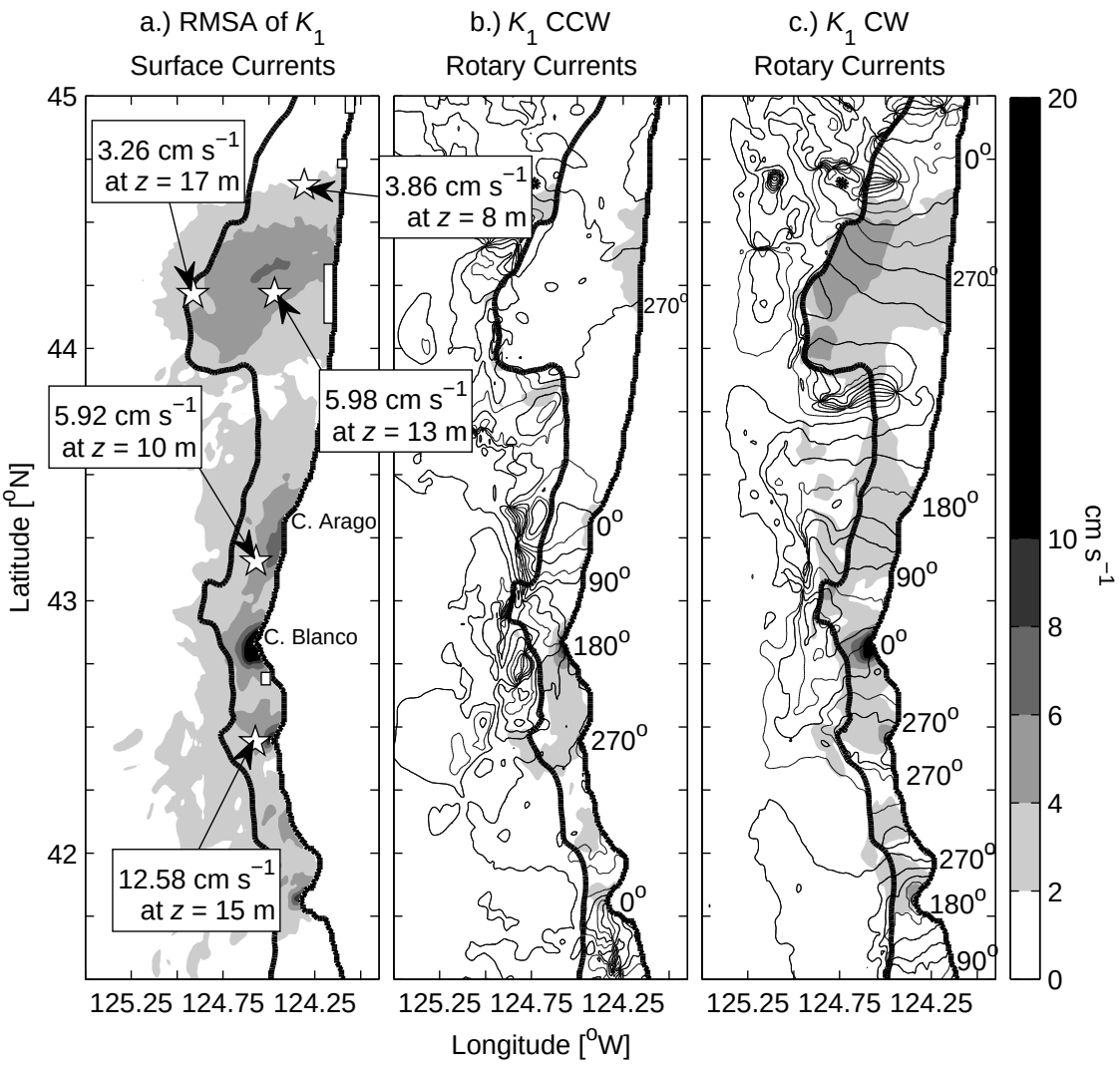

FIG. 3. (a) K_1 RMSA along the Oregon coast from case TW. Stars mark 2001 (along 44.3°N, 44.75°N) and 2002 (near Cape Blanco) mooring locations, with annotations giving the moorings' K_1 RMSA at their surface-most depth bin. White boxes along the coast at 42.7°N, $44.1 - 44.25$°N, 44.75°N , and 45°N mark proposed and pilot marine protected areas and reserves. (b) Counterclockwise rotary current amplitude (shading) and phase (thin lines, every 30°) of depth-averaged K_1 currents. (c) Clockwise rotary current amplitude and phase of depth-averaged K_1 currents. In all panels, the thick black line marks the 200-m isobath.

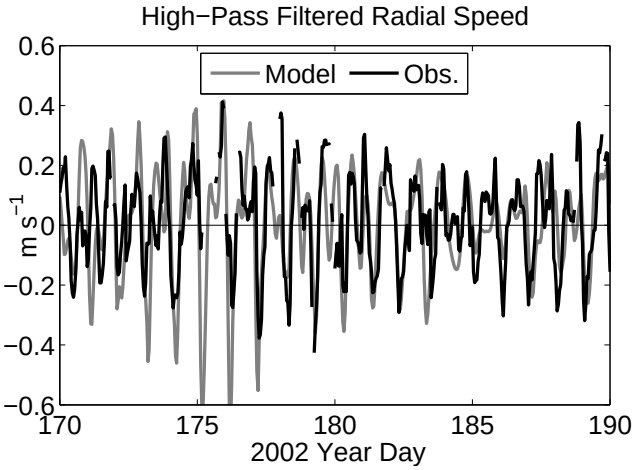

FIG. 4. Time series of HFR-observed (black) and model (gray) radial velocity component near Cape Blanco (location marked in inset in Figure 5b).

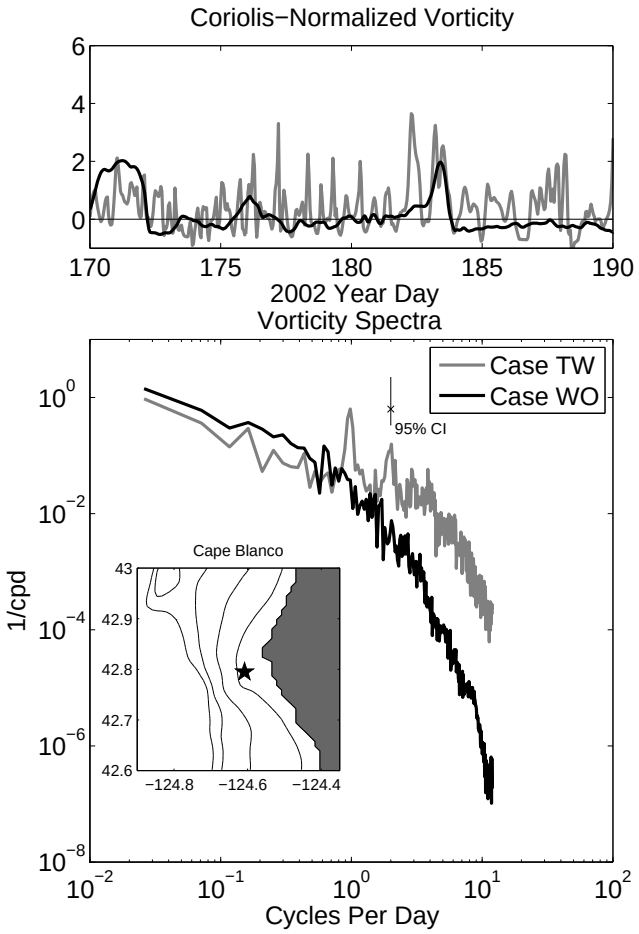

FIG. 5. Upper: Time series of Coriolis-normalized relative vorticity from case WO (black) and case TW (gray) during the same time period from near Cape Blanco. Lower: Spectra of vorticity time series from case WO (black) and case TW (gray), as computed from the entire model run. The 95% confidence interval is shown. Inset: Close-up of Cape Blanco region. Star marks the location of the time series in Figure 4 and this figure. Black lines mark the 50-, 100-, 150-, and 200-m isobaths.